Hybrid incompatibility emerges at the one-cell stage in interspecies *Caenorhabditis* embryos

Jessica Bloom[1], Rebecca Green[2*], Arshad Desai[2,3], Karen Oegema[2,3], Scott A. Rifkin[1**@]

1 Department of Ecology, Behavior, and Evolution, School of Biological Sciences, University of California, San Diego, La Jolla, CA 92093, USA

2 Department of Cell and Developmental Biology, School of Biological Sciences, University of California, San Diego, La Jolla, CA 92093, USA

3 Department of Cellular and Molecular Medicine, University of California San Diego, La Jolla, California 92093, USA.

@ Lead Contact: Scott A. Rifkin (sarifkin@ucsd.edu)

*Corresponding authors: Scott A. Rifkin (sarifkin@ucsd.edu), Rebecca Green (regreen@ucsd.edu)

SUMMARY:

Intrinsic reproductive isolation occurs when genetic differences between populations disrupt the development of hybrid organisms, preventing gene flow and enforcing speciation.[1–4] While prior studies have examined the genetic origins of hybrid incompatibility,[5–18] the effects of incompatible factors on development remain poorly understood. Here, we investigate the mechanistic basis of hybrid incompatibility in *Caenorhabditis* nematodes by capitalizing on the ability of *C. brenneri* females to produce embryos after mating with males from several other species. Contrary to expectations, hybrid incompatibility was evident immediately after fertilization, suggesting that post-fertilization barriers to hybridization originate from physical incompatibility between sperm and oocyte-derived factors rather than from zygotic transcription, which starts after the 4-cell stage.[19–22] Sperm deliver chromatin, which expands to form a pronucleus, and a pair of centrioles, which form centrosomes that attach to the sperm-derived pronucleus and signal to establish the embryo's anterior-posterior axis.[23,24] In *C. brenneri* oocytes fertilized with *C. elegans* sperm, sperm pronuclear expansion was compromised, frequent centrosome detachment was observed, and cortical polarity was disrupted. Live imaging revealed that defective polar body extrusion contributes to defects in mitotic spindle morphology. *C. brenneri* oocytes fertilized with *C. remanei* or *C. sp. 48* sperm showed similar defects, and their severity and frequency increased with phylogenetic distance. Defective expansion of the sperm-derived pronucleus and unreliable polar body extrusion immediately after fertilization generally underlie the inviability of hybrid embryos in this clade. These results indicate that physical mismatches between sperm and oocyte-derived structures may be a primary mechanism of hybrid incompatibility.

KEYWORDS: intrinsic reproductive isolation, hybrid incompatibility, Caenorhabditis nematodes, cell polarity, nuclear size, centrosome attachment, mitotic spindle, polar body extrusion

RESULTS AND DISCUSSION

Hybrid embryos of *C. brenneri* females and *C. elegans* males exhibit polarity defects prior to zygotic genome activation

Prior work has shown that *C. brenneri* females can be fertilized by males from different species across the *Elegans* subgroup (confirmed species in dark grey in **Fig. 1A**), although the resulting hybrid embryos inevitably die (**Fig. 1A**).[25–27] To identify the incompatibilities that prevent successful embryonic development, we analyzed *C. brenneri* oocytes fertilized with *C. elegans* sperm, which allows us to take advantage of tools available in *C. elegans*. Brood size, especially on the second day after mating, was consistently smaller in the interspecies cross than for an intraspecies cross of *C. brenneri* (**Fig. 1B**), suggesting that either fewer sperm are transferred in the interspecies cross or that the ability of sperm to remain fertilization competent in the spermatheca is reduced. As anticipated, all of the hybrid embryos died, compared to only 6% (145/2263 embryos) and 2% (56/2991 embryos) respectively, of the intraspecies fertilized *C. brenneri* and *C. elegans* embryos (**Fig. 1B**).

Prior work has shown that mismatches in the timing and regulation of zygotic gene expression from two divergent genomes can lead to hybrid incompatibility.[13,14,28,29] However, problems could also arise before the onset of zygotic gene expression due to incompatibilities between the interacting components of oocytes and sperm. Based on work in *C. elegans* and other *Caenorhabditis* species, we expect zygotic genome activation to begin at the 4-cell stage (**Fig. 1C**).[19–22] A previous investigation showed that hybrid *Caenorhabditis* arrest throughout embryogenesis.[25] To determine when incompatibility first becomes evident, we mated unmarked *C. brenneri* or *C. elegans* (*fog-2*) females to males from a *C. elegans* strain in which the genome encodes fluorescent reporters that mark nuclei in the endoderm (*green*), mesoderm (*yellow*), and ectoderm (*red*)[30,31] (**Fig. S1A**). We also mated unmarked *C. brenneri* males to *C. brenneri* females for comparison. Since the markers do not turn on until later in development, embryos were initially filmed using differential interference contrast microscopy to monitor events between fertilization and the 4-cell stage (**Fig. 1D-E**). Embryos were then left to develop overnight

and imaged the next day to identify the point of arrest and determine whether the tissue-specific markers had turned on (**Fig. S1A-C**).

Events between fertilization and the 4-cell stage in *C. elegans* (schematized in **Fig. 1C**) have been extensively studied.[24,32,33] As is typical for metazoans, oocytes lack centrioles/centrosomes[34,35] and the sperm brings a pair of centrioles, along with the paternal chromatin, into the oocyte. The maternal chromatin completes two rounds of meiotic segregation at the anterior end of the embryo to generate two polar bodies and the maternal pronucleus, while the sperm chromatin and centrioles remain quiescent as a compact unit. After the second polar body has been jettisoned, the sperm centrioles recruit a microtubule-nucleating scaffold to form centrosomes, and the pronucleus that has formed around the sperm chromatin begins to expand.[36–38] The nascent centrosomes stay associated with the sperm pronucleus and are sandwiched between the pronucleus and the cortex. The centrosomes send a signal that marks the embryo posterior, which triggers the formation of two antagonistic cortical domains: a posterior domain containing a PAR ("Partitioning-defective") protein complex that includes PAR-2 and an anterior domain containing a PAR protein complex that includes PAR-6 (**Fig. 1D**).[23,24,39–41] The first mitotic spindle divides the embryo between these two domains, generating a larger anterior (AB) cell and smaller posterior (P1) cell. During the second cell division, the spindle in the anterior AB cell sets up vertically (perpendicular to the anterior-posterior axis of the embryo), and the spindle in the posterior P1 cell sets up horizontally (parallel to the anterior-posterior axis of the embryo), which leads to a characteristic organization of the daughters of AB (ABa and ABp) and P1 (P2 and EMS) at the 4-cell stage (ABa on top of EMS in the middle flanked by ABp and P2 on the anterior and posterior sides; **Fig. 1C,D**).[24] Improper organization disrupts cell-cell signaling and cell-fate specification.

In *C. elegans*, knocking down *par-2,* by RNAi, prevents a functional posterior domain from forming, and the spindles in both daughter cells line up vertically (as they would in the anterior AB cell), leading to a 4-leaf clover-like organization at the 4-cell stage (Both Anterior; **Fig.1D, Fig. S1D**).[24,39,40,42,43] Knocking down *par-6* prevents the formation of a functional anterior domain and causes the spindles in both daughter cells to line up horizontally (as they would in the posterior P1 cell), leading to a linear chain of

cells at the 4-cell stage (Both Posterior; **Fig. 1D, Fig. S1D**).[39,40,42] Similar polarity defects were observed in *C. brenneri* embryos after RNAi of *par-2* and *par-6*, although the *par-6* knockdown led to roughly equivalent numbers of embryos with Both Anterior and Both Posterior phenotypes (**Fig. 1D, Fig. S1D**; **Video S1**). Whereas intraspecies *C. brenneri* and *C. elegans* embryos exhibited a normal 4-cell pattern in 92% (12/13) or 95% (19/20) of cases, respectively, only 7% (3/44) of hybrid embryos resulting from mating *C. elegans* males with *C. brenneri* females did. Instead, 21% (9/44) of hybrid embryos exhibited a Both Anterior phenotype, 9% (4/44) exhibited a Both Posterior phenotype, and 64% (28/44) displayed an aberrant pattern (Other) that typically included an abnormally positioned P1 cell (**Fig. 1E**). To more directly probe polarity establishment in hybrids, we identified a *C. elegans* anti-PAR-2 antibody[44] that also detects the posterior cortical domain in 1-cell stage *C. brenneri* embryos (25/25). Consistent with a polarity defect, hybrid embryos either completely lacked a defined PAR-2 domain (3/9) or exhibited an incomplete or misplaced PAR-2 domain (5/9), with only one example establishing a proper PAR-2 domain (**Fig. 1F**).

To determine whether polarity problems affected the ability of hybrid embryos to reach mid-embryogenesis and turn on tissue-specific markers, we collected DIC and spinning disk confocal fluorescence z-stacks the next day, after the embryos had died (**Fig. S1A-C**). This revealed that the organization of the embryos at the 4-cell stage predicted whether they went on to express the fluorescent germ-layer reporters. Of the three hybrid embryos that exhibited normal morphology at the 4-cell stage, all turned on the germ layer reporters prior to arrest. By contrast, only 11% (1/9) of hybrids exhibiting a Both Anterior polarity phenotype, 25% (1/4) of hybrids exhibiting a Both Posterior polarity phenotype, and 38% (10/26) of hybrids exhibiting an Other aberrant 4-cell morphology defect turned on the germ layer reporters prior to arrest (**Fig. S1A-C**). We conclude that hybrid embryos from matings between *C. elegans* males and *C. brenneri* females exhibit problems with cell patterning consistent with a failure to properly establish anterior-posterior polarity and that these polarity defects lead to an inability to properly pattern tissues that express germ layer reporters. Polarity defects are evident prior to zygotic genome activation, suggesting that they arise due to an incompatibility between the components of the oocyte and sperm.

Centrioles detach from the sperm pronucleus in hybrid embryos, likely due to delayed sperm pronuclear expansion

Next, we wanted to understand the nature of the incompatibility that gives rise to the polarity defects in hybrid embryos. Cortical polarity is established at the one-cell stage when the sperm-provided centrioles recruit a pericentriolar material (PCM) scaffold composed of SPD-5. This scaffold recruits γ-tubulin complexes for microtubule nucleation and provides a cue that establishes cortical polarity (**Fig. 2A**).[23,45–47] To determine if sperm-provided *C. elegans* centrioles recruit a PCM scaffold in *C. brenneri* oocytes, we used immunofluorescence to visualize both γ-tubulin, which docks onto the SPD-5 scaffold (**Fig. 2B; Fig. S2A,A'**),[46,48] and α-tubulin, to monitor microtubule nucleation (**Fig. S2B**). In both *C. elegans* (12/12) and *C. brenneri* (14/14) embryos, centrosomes adjacent to the sperm pronucleus recruited γ-tubulin, and α-tubulin-containing microtubules emanated from the centrosomes **Fig. 2B; Fig. S2A).** In hybrid embryos, centrosomes also recruited γ-tubulin and nucleated α-tubulin-containing microtubules (**Fig. 2B**; **Fig. S2A**;12/12 embryos), indicating that the centrioles from *C. elegans* sperm can form centrosomes that nucleate microtubules in *C. brenneri* oocytes. In *C. elegans* and *C. brenneri*, both centrosomes remain attached to the sperm pronucleus. However, in the hybrids one or both centrosomes frequently detached from the sperm-derived pronucleus (**Fig. 2B**; **Fig. S2A**; 11/12 embryos).

Centrosome detachment in hybrid embryos has the potential to disrupt polarity establishment by preventing the sperm pronucleus from holding the centrosomes in a position adjacent to the cortex, where they deposit the polarity cue. Proper centrosome positioning is also important for establishing spindle structure and orientation.[49,50] To investigate centrosome detachment further, centrosome movement was tracked in living embryos. Unmarked *C. brenneri* or *C. elegans* (*fog-2*) females were mated to males from a *C. elegans* strain expressing an mCherry fusion with the centriolar protein SAS-4 (mCherry centrioles).[48] Unmarked *C. brenneri* males were also mated to *C. brenneri* females as a control. In the *C. elegans* embryos, during the interval when polarity establishment occurs,[23,36,39] the two mCherry::SAS-4

marked centrosomes separated as the sperm pronucleus came into proximity to the cortex (**Fig. 2C,D**). Throughout this process, both centrosomes remained attached to the sperm pronucleus (Pronuclear Appearance stage; 24/26 embryos; **Fig. 2C,D, Video S2**). Centrosome-pronuclear attachment is mediated by dynein anchored to the pronuclear envelope via the LINC complex,[51–53] which pulls the centrosomes towards the pronuclei by walking towards the minus ends of centrosomally nucleated microtubules. After polarity establishment, the sperm and oocyte pronuclei migrated toward each other as the dynein associated with the oocyte pronucleus captured and walked toward the minus ends of the centrosomal microtubules.[51,53] At pronuclear meeting, the centrosomes in the *C. elegans* embryos were positioned above and below the interface between the pronuclei (**Fig. 2E**, Pronuclear Meeting; 25/26 embryos; **Video S2**). Upon pronuclear envelope break-down, the first mitotic spindle formed along the embryo's long axis, with the mCherry-containing centrosomes at the two spindle poles (**Fig. S2B, Video S2**). After the cell divided, each daughter cell inherited a centrosome with a single sperm-derived centriole (**Fig. S2B, Video S2;** 26/26 embryos).

In contrast, at the pronuclear appearance stage in hybrid embryos, one of the two mCherry-containing centrosomes frequently detached (>9 μm of separation) from the sperm pronucleus and migrated into the cytoplasm or along the cortex (12/15 embryos; **Fig. 2D**). The detached centrosomes were often recaptured prior to or during pronuclear meeting (**Video S2**). Even though centrosomes were recaptured, in 67% of cases (10/15), the centrosomes were improperly positioned relative to the two pronuclei prior to nuclear envelope breakdown (**Fig. 2E**).

Similar phenotypes in which one centrosome detaches from the sperm pronucleus and subsequently reattaches prior to pronuclear meeting have been observed following perturbations that reduce the surface area of the sperm pronucleus.[49,54] Experimental data support the idea that the number of centrosomes that can attach to a pronucleus is limited by its surface area. Small pronuclei can only interact with the microtubules from one centrosome, and interaction with microtubules from a second centrosome becomes possible only after pronuclei pass a threshold size.[54] To determine if the size of the

sperm pronucleus in hybrids could be the cause of centrosome detachment, we measured the cross-sectional area of the sperm and oocyte pronuclei at pronuclear appearance and pronuclear meeting. At pronuclear appearance, the sperm pronuclei in hybrids were about half the size of those in intraspecies *C. brenneri* and *C. elegans* embryos (**Fig. 2F**). At pronuclear meeting, the hybrid sperm pronuclei remained about half the size of their intraspecies counterparts and of the oocyte pronuclei (**Fig. 2F; Fig. S2C**). Even if the second centrosome eventually reattached to either the sperm or oocyte pronucleus, the arrangements of both the centrosomes and pronuclei were abnormal at pronuclei meeting (**Fig. 2E,F**). Thus, the *C. elegans* sperm-derived pronucleus is unable to properly expand in the *C. brenneri* oocyte cytoplasm, which likely leads to centrosome detachment from the nucleus and polarity defects.

Improperly positioned centrosomes cause defects in spindle orientation, and failures of polar body extrusion lead to abnormal spindle morphology

Centrosomes are responsible for building the mitotic spindle, thus aberrant centrosome-pronuclear arrangements at the point of pronuclear meeting could lead to spindle structure defects after nuclear envelope breakdown. Embryonic polarity defects could also contribute to spindle orientation problems (**Fig. 3A**).[49,50,55] To analyze spindle orientation, we measured the angle between the centrosome-to-centrosome axis of the spindle and the anterior-posterior axis of the embryo using DIC microscopy (**Fig. 3B**); in DIC images, centrosomes appear as clear areas, devoid of yolk particles. For this analysis, we collected images every 30-45 seconds for 3.5-4.5 minutes starting from the onset of metaphase. Whereas 95% (161/168) of spindle orientations were between -7.5° and 10.6° of the anterior-posterior axis in control embryos, only 37% were in this range for hybrid embryos, which instead exhibited spindle angles between -56° and 51°. The spindle orientation problems in hybrid embryos are consistent with the defects in cortical polarity (**Fig. 1E**), which is associated with large oscillations off the longitudinal axis at anaphase.[55]

To visualize spindle structure, we mated unmarked *C. brenneri* or *C. elegans* (*fog-2*) females to males from a *C. elegans* strain expressing the mCherry-tagged centriolar protein SAS-4 as before and dissected the worms into media containing SiR-Tubulin, a vital dye that stains microtubules. *C. elegans* and *C. brenneri* embryos had centrosomal microtubule asters at the two spindle poles and robust arrays of kinetochore microtubules pointed toward the centrally-aligned chromosomes (**Fig. 3C,D, Video S3**). In hybrids, 19/22 hybrid embryos exhibited abnormal spindle morphologies. These included arrays of kinetochore microtubules (spindle arms) that pointed in random directions instead of towards the other centrosome, most likely because the centrosome was attempting to capture chromosomes that were in an atypical position when nuclear envelope breakdown occurred (**Fig. 3C,D**; **Fig. S2C; Video S3**). In 8/22 of hybrid embryos, the mitotic spindle microtubules appeared to capture remnants of the meiotic spindle in the anterior of the embryo that had segregated the oocyte-derived chromosomes into the polar body (**Fig. 3C,D**). In these cases, the mitotic spindle appeared to pull a part of the meiotic spindle into the cytoplasm and/or to engage meiotic chromosomes. The continued presence of the meiotic spindle in the mitotic cytoplasm, suggests that embryo failed to successfully jettison of one set of sister chromatids into the 2nd polar body at the end of meiosis II.[56] We also analyzed spindles by immunofluorescence, staining for γ-tubulin and microtubules and confirmed the presence of spindles with anomalous morphology (7/15 embryos). We frequently observed chromosomes surrounding the centrosomal asters (10/15 embryos; **Fig 3E**) in hybrids and never in *C. elegans* or *C. brenneri* embryos. These chromosomes had a morphology consistent with meiotic chromosomes, supporting the conclusion that extrusion of the 2nd polar body frequently fails in hybrid embryos and leads to defects in spindle morphology.

A similar suite of early defects is observed in hybrid embryos generated by crosses between *C. brenneri* females and males from three Elegans group species

The work above has shown that the inviability of hybrids from female *C. brenneri* and male *C. elegans* starts with problematic interactions between the components of the oocyte and sperm at fertilization, well before mis-regulation of zygotic gene expression. In addition to *C. elegans*, C*. brenneri*

females are able to be fertilized by males of many other species in the *Caenorhabditis Elegans* subgroup.[25,26] Nearly all of these hybrid offspring die during embryogenesis, which is common for hybrids between various *Caenorhabditis* species.[25,26] To determine whether the fatal incompatibilities are different for each species pair and whether the severity of the developmental defects increase with phylogenetic distance, we analyzed hybrid embryos from two additional crosses to *C. brenneri* females: *C. sp. 48* and *C. remanei*. *C. brenneri* and *C. elegans* are separated by around 200 million generations (or around 35 million years of evolution), although these estimates have wide uncertainty.[57] *C. sp. 48* is a sister species of *C. brenneri*, about a third as divergent at the amino acid level from *C. brenneri* as *C. elegans*. *C. remanei* has a more recent common ancestor with *C. brenneri* than *C. elegans*, but its protein sequences are on average around 17% more divergent (**Fig. 4A**). Compared to intraspecies crosses, *C. brenneri* females had a reduced brood size after mating with *C. remanei*, and, although nearly all embryos died, a few were able to hatch (2/887) (**Fig. 4B**). *C. brenneri* females crossed to *C. sp. 48* males had brood sizes comparable to intraspecies crosses, but the resulting embryos all died during embryogenesis (**Fig. 4B**).

To document the range of early embryonic defects, we scored DIC movies of ~120 embryos from *C. brenneri, C. sp. 48, C. remanei*, and *C. elegans* as well as hybrids between *C. brenneri* females and the three other species for the presence of 20 distinct early embryonic defects (**Fig. 4C,D; Fig. S3A, Table S1**). All of the hybrid embryos exhibited a similar spectrum of early defects, including small and/or misshapen sperm pronuclei, centrosome detachment, and a “cross-eyed” phenotype indicative of chromosome mis-segregation.[49] We also observed evenly sized AB and P1 cells at the 2-cell stage and abnormal cell patterns at the 4-cell stage indicative of cell polarity defects (**Video S4)**. Defects in the more distant *C. remanei* and *C. elegans* crosses were more frequent and severe compared to the sister species cross and included failures of both polar body extrusion and cytokinesis.

Conclusion

Incompatibility between interacting components in the oocytes and sperm may be a common mechanism underlying hybrid incompatibility between nematodes of the *Caenorhabditis Elegans* subgroup (**Fig. 4E)**. A major driver of sperm incompatibility with *C. brenneri* oocytes is a delay in expanding the sperm-derived pronucleus. Prior work suggests that a small sperm pronucleus would lead to centrosome detachment,[49,54] which we frequently observed in hybrid embryos. Centrosome detachment, in turn, could cause the observed defects in cell polarity (**Fig. 4F**). It is also possible that the microtubule asters of detached centrosomes may aberrantly capture the meiosis II spindle, leading to the polar body extrusion defects we observed. It will be interesting to see if delayed expansion of the sperm-derived pronucleus is a feature specific to hybrids with *C. brenneri* females, which might be a valuable adaptation for a species that tolerates promiscuous fertilization, or whether it is a more general feature of hybrids between different species pairs across the *Elegans* group.

The fact that *C. brenneri*/*C. sp. 48* hybrids often overcome their initial problems to reach a superficially normal 4-cell stage (**Fig. 4D**), suggests that while there are incompatibilities that destabilize early development, the severity of destabilization increases with greater evolutionary distance between the parents. The variability in development between hybrid embryos, even within a cross, is consistent with the idea that many developmental events are less robust in hybrids than in intraspecies embryos and fail at appreciable frequency. Although a few hybrid embryos may thread the needle to find a narrow pathway to hatching, most fall victim to a series of stochastic failures that build on each other to a fatal outcome (**Fig. 4F**). These failures that cause hybrid incompatibility begin in the zygote almost immediately after fertilization and well before the activation of developmental gene expression programs.

ACKNOWLEDGEMENTS

We would like to thank members of the Rifkin, Oegema, and Desai labs for helpful discussions. We would like to thank the Hyman lab for the generous gift of the PAR-2 antibody and Marie-Anne Félix for the generous gift of strain BRC20359 (*C. sp. 48*). We would also like to thank Anthony Ye and Aidan Linkins for their help. This work was supported by grants from the NIH (GM103782) and the NSF IOS (1936674) to S.A.R. and from the NIH to K.O. (GM147265). A.D. and K.O. received salary and other support from the Ludwig Institute for Cancer Research. JB was partially supported by NIH/NIGMS (T32 GM127235). Some strains were provided by the CGC, which is funded by NIH Office of Research Infrastructure Programs (P40 OD010440).

AUTHOR CONTRIBUTIONS

Conceptualization: J.B., R.G., K.O., S.A.R.; Methodology: J.B., R.G., K.O., S.A.R.; Formal analysis: J.B., R.G.; Investigation: J.B., R.G.; Resources: S.A.R., K.O.; Data curation: J.B., R.G.; Writing - original draft: J.B., R.G., K.O., S.A.R.; Writing - review & editing: J.B., R.G., A.D., K.O., S.A.R.; Visualization: J.B., R.G.; Supervision: R.G., S.A.R., K.O.; Project administration: S.A.R., K.O.; Funding acquisition: S.A.R., K.O.

DECLARATION OF INTERESTS

The authors declare no competing interests.

281 **MAIN FIGURES WITH TITLES AND LEGENDS**

Bloom et al., Figure 1

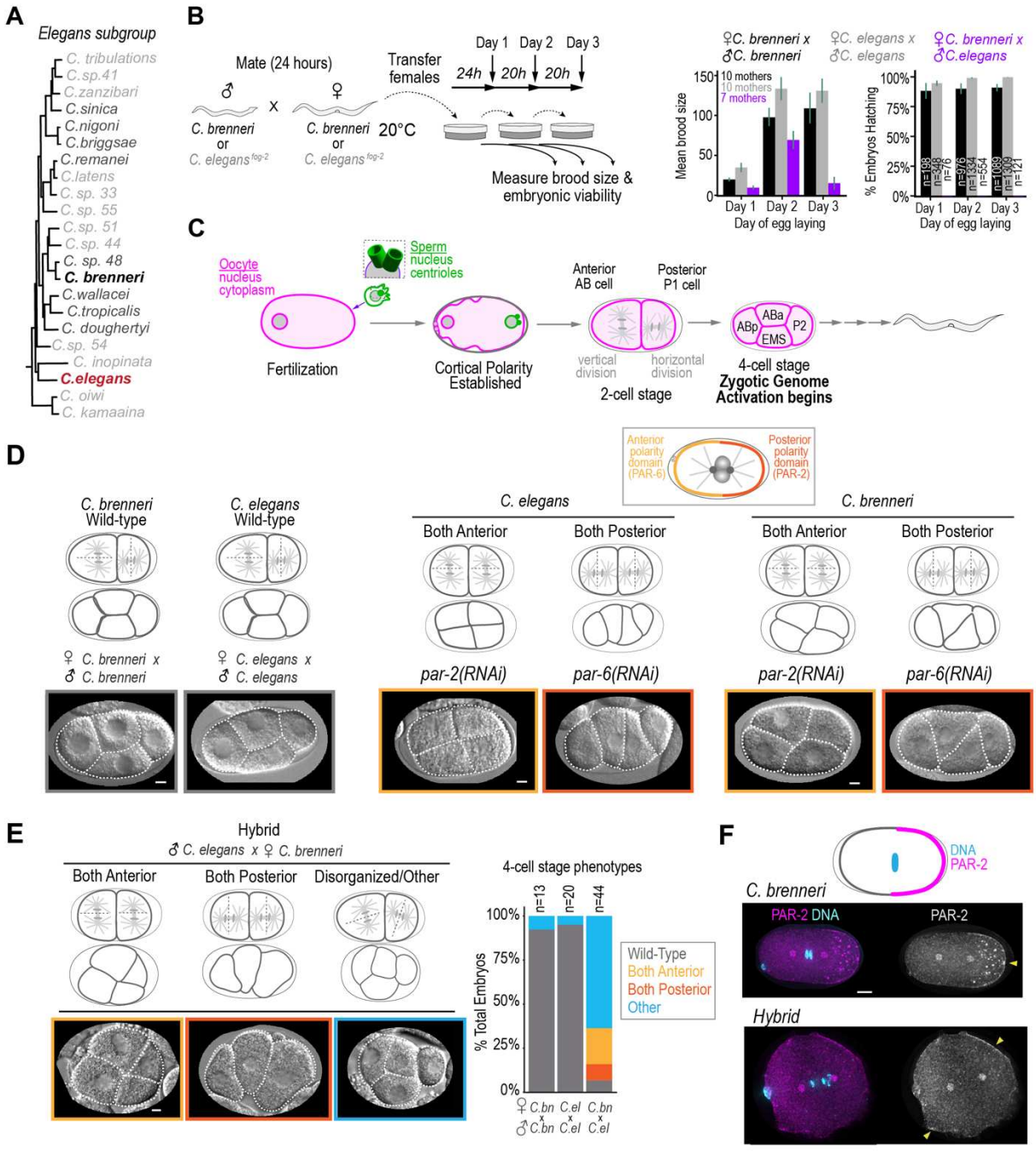

282

Figure 1. **Hybrid embryos resulting from fertilization of *C. brenneri* oocytes with *C. elegans* sperm exhibit polarity defects prior to zygotic genome activation.** (**A**) Phylogeny of the *Caenorhabditis* Elegans subgroup. *C. brenneri* females have been shown to be cross-fertile with *C. elegans* (*red*) males and males from the species marked in dark grey. (**B**) Schematic illustrating how embryos were collected after mating. Graphs show the average brood size and % hatching for the embryos collected during each day of egg laying. Day 1 is 0-24 hours post-mating; day 2 is 24-44 hours post-mating; day 3 is 44-64 hours post-mating. n refers to the number of embryos counted per cross. Error bars are ± SE. **(C)** Schematic of the events between fertilization and the 4-cell stage when Zygotic Genome Activation (ZGA) begins. The sperm brings in a pair of centrioles along with the sperm chromatin into the oocyte. Hybrid incompatibility could arise due to misregulation of gene expression after ZGA or before ZGA, due to incompatibilities between the structural components of sperm and oocyte. (**D**) Differential interference contrast (DIC) images of 4-cell stage embryos are shown for: (*left*) control intraspecies *C. brenneri* and *C. elegans* embryos; (*middle*) *par-2(RNAi)* and *par-6(RNAi) C. elegans* embryos; and (*right*) and *par-2(RNAi)* and *par-6(RNAi) C. brenneri* embryos. For phenotypic quantification see *Fig. S1D*. The schematic on top illustrates the anterior PAR-6 (*yellow*) and posterior PAR-2 (*orange*) domains at the 1-cell stage in *C. elegans*. Schematics immediately above the images show the expected cell and spindle orientations for two-cell and four-cell stage embryos for each condition. (**E**) DIC images illustrating the three non-wild-type classes of 4-cell stage phenotypes observed for hybrid embryos resulting from mating *C. brenneri* females with *C. elegans* males (Both Anterior, Both Posterior, and Disorganized/Other). Schematics above the images illustrate the cell and spindle orientations at the two-cell and four-cell stages for each embryo. The graph quantifies the percentage of embryos that appeared wild-type or exhibited each phenotype. (**F**) (*top*) Schematic illustrating the localization of PAR-2 and DNA in a control embryo. **(***left***)** Representative immunofluorescence images of *C. brenneri* (top; n = 25) and hybrid embryos (bottom; n = 9) stained for PAR-2 (*magenta*) and DNA (*cyan*). (*right*) Grayscale PAR-2 images with yellow arrowheads marking the PAR-2 domains. Scale bars represent 5μm.

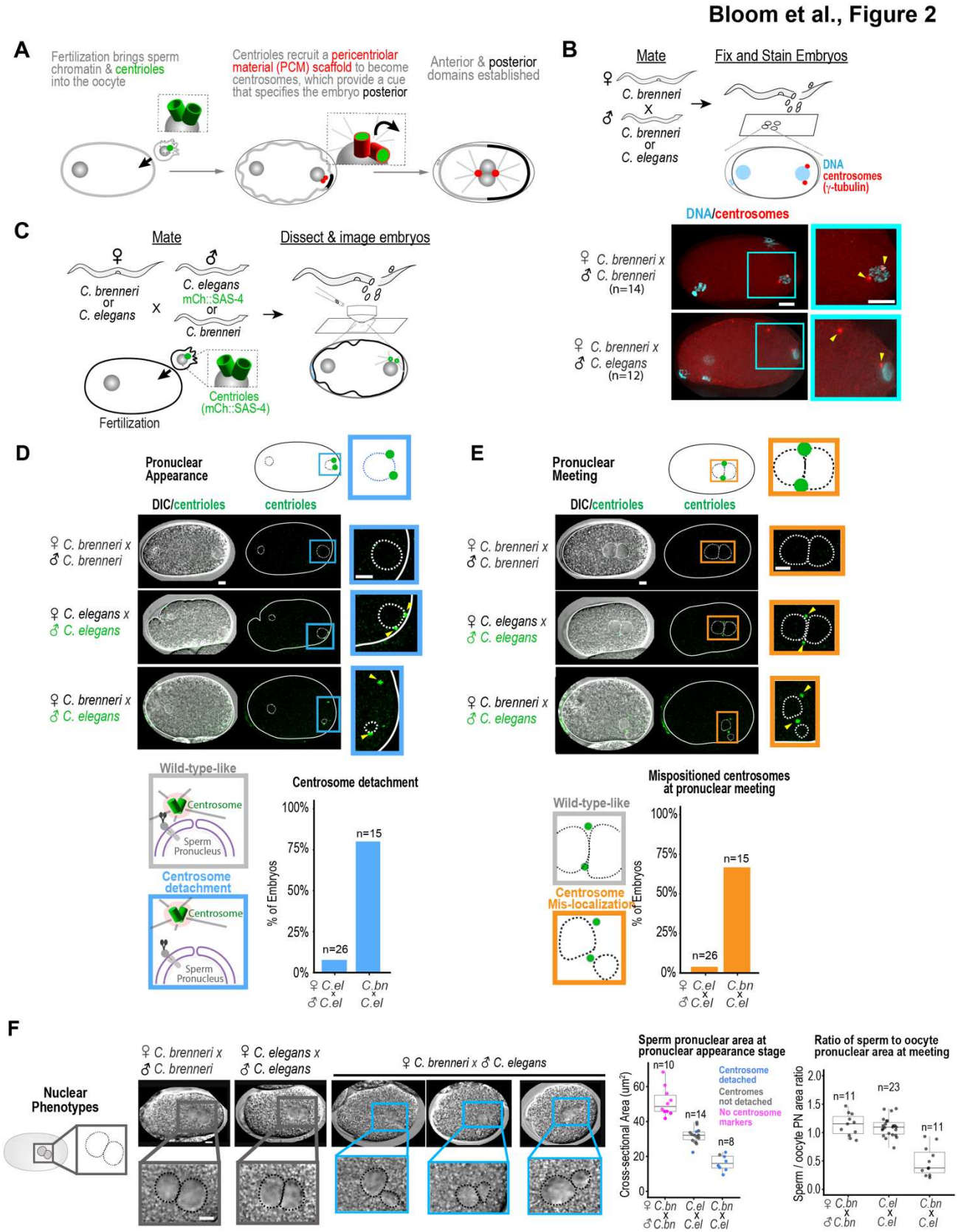

306

Figure 2. ***Centrioles detach from the sperm pronucleus in hybrid embryos, likely due to delayed sperm pronuclear expansion.*** (**A**) The schematic illustrates how fertilization triggers polarity establishment in the 1-cell embryo. The sperm brings in a pair of centrioles (*green*) that are converted to centrosomes (*red*) via the recruitment of the PCM scaffold protein SPD-5 from the oocyte cytoplasm. The centrosomes, which are sandwiched between the sperm pronucleus and the cortex, provide a cue that specifies the embryo posterior. (**B**) (*top*) The schematic illustrates the mating regime and markers shown in the immunofluorescence images below. (*bottom*) Representative images of 1-cell stage *C. brenneri* (n = 14) and hybrid (n = 12) embryos after the conversion of centrioles to centrosomes, but prior to pronuclear migration, stained for DNA (cyan) and γ-tubulin (red). Insets are magnified 1.7X. γ-tubulin (red) is scaled equivalently in the two images. (**C**) The schematic illustrates the mating of *C. brenneri* or *C. elegans* females with *C. elegans* males whose centrioles are stably marked with mCherry::SAS-4 (*green*) to allow monitoring of sperm centriole position throughout the first cell division. (**D**) (*Top*) Paired DIC/fluorescence overlay (*left*) and fluorescence-only (*right*) images of *C. brenneri*, *C. elegans,* and hybrid pronuclear appearance stage 1-cell embryos. The schematic on top illustrates the expected position of the mCherry::SAS-4 marked centrioles adjacent to the sperm pronucleus (*green*). The white solid lines trace the embryo. The white dashed lines trace pronuclei in DIC and fluorescence images. Insets are magnified 2.3X, and yellow arrowheads mark centrosomes. Image intensities for centrioles are scaled to highlight centriole position and cannot be compared across images. (*Bottom*, *left*) The schematics depict wild-type-like attachment (*grey box*) and aberrant detachment (*blue box*) of centrosomes from the sperm pronucleus. (*Bottom*, *right*) The graph quantifies the percentage of embryos with centriole detachment (>9 μm separation) from the sperm pronucleus. (**E**) (*Top*) Paired DIC/fluorescence overlay (*left*) and fluorescence-only (*right*) images of *C. brenneri*, *C. elegans,* and hybrid pronuclear meeting stage 1-cell embryos. The schematic on top illustrates the expected position of the mCherry::SAS-4 marked centrioles (*green*) above and below the interface between the maternal and paternal pronuclei. The white solid lines trace the embryo. The white dashed lines trace pronuclei in DIC and fluorescence images. Insets are magnified 2.3X, and yellow arrowheads mark centrosomes. Image intensities are scaled to highlight centriole localization and cannot be compared across images. (*Bottom*, *left*) The schematics depict wild-type-like positioning of the centrosomes above and below the interface between the maternal and paternal pronuclei (*grey box*) and mispositioning of the centrosomes and nuclei (*orange box*). (*Bottom*, *right*) The graph quantifies the percentage of embryos with mispositioned centrosomes at pronuclear meeting. (**F**) DIC images of representative *C. brenneri*, *C. elegans*, and *hybrid* embryos at pronuclear meeting. Insets are magnified 2X (the black dotted lines trace pronuclei). The left graph plots the cross-sectional area of sperm pronuclei at the pronuclear appearance stage. Median (IQR) for sperm pronuclear cross-sectional area is 49 (39-58), 32 (28-37), and 16 (9-23) μm^2 for *C. brenneri*, *C. elegans*, and hybrid embryos, respectively. Centriole detachment is indicated by blue circles, and wild-type-like centriole separation is indicated by gray circles. In *C. brenneri*, centrioles were not labeled and detachment was not scored (*pink circles*). The right graph plots the ratio of sperm to oocyte pronuclear area at pronuclear meeting (also see *Fig. S2C*). Median (IQR) for sperm pronuclear area to oocyte pronuclear area is 1.2 (0.9-1.5), 1.1 (0.9-1,3), 0.4 (0.01-0.73) for *C. brenneri*, *C. elegans*, and hybrid embryos, respectively. Scale bars represent 5μm.

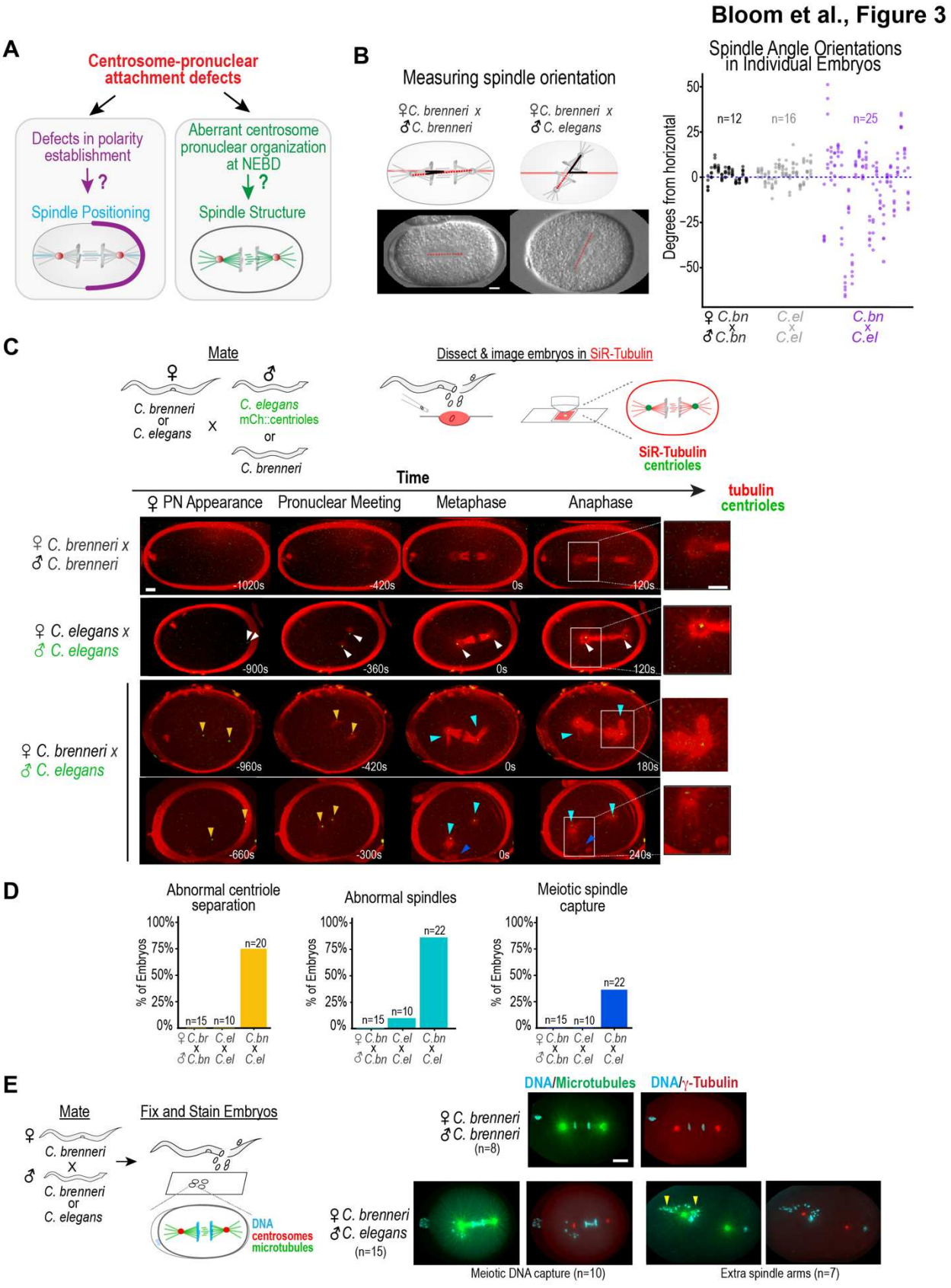

344

Figure 3. *Caenorhabditis* hybrid embryos exhibit defects in spindle orientation, polar body extrusion, and spindle morphology (**A**) A schematic illustrating how detachment of centrosomes from the sperm pronucleus could contribute to defects in polarity establishment, spindle positioning, and spindle morphology in the early embryo. (**B**) Schematics (*top*) and images (*bottom*) illustrating how spindle orientation was assessed. At each timepoint, the angle between the centrosome-to-centrosome axis of the spindle (red dashed line) and the anterior-posterior axis of the embryo (red solid line) was measured. For each embryo six measurements were made at 30-45s intervals starting at metaphase. The graph plots the six measured angles for each embryo in a vertical row. Angles were measured in *C. brenneri* (*black*), *C. elegans* (gray) or hybrid (*purple*) embryos. (**C**) (*Top*) A schematic illustrating how *C. brenneri* or *C. elegans* females were mated with *C. elegans* males with mCherry::SAS-4-marked centrioles to enable live tracking of centrioles (*green*). *C. brenneri* females were also mated with *C. brenneri* males as a control. Embryos were dissected into the vital dye SiR-Tubulin (*red*) to monitor microtubules. Images are maximum intensity projections of representative intraspecies *C. brenneri* and *C. elegans* embryos and hybrids. Times are seconds relative to metaphase. White and yellow arrows indicate proper or improper centriole separation, respectively. Cyan arrows indicate abnormal spindle morphology. Dark blue arrows indicate meiotic DNA capture. Insets (right) show 2X magnifications of one anaphase spindle pole as indicated. Maximum intensity projections were made of all z-planes containing the centrosomes and spindle structures, and SiR-Tubulin intensities were scaled to best show spindle morphology and cannot be directly compared. (**D**) The graphs quantify the percentage of embryos exhibiting abnormal centriole separation (*yellow*), abnormal spindle morphology (*cyan*), and meiotic DNA capture (*blue*) for the indicated conditions. (**E**) (*Left*) The schematic illustrates the mating regime and markers shown in the immunofluorescence images to the right. (*Right*) Representative immunofluorescence images of *C. brenneri* (n = 8) and hybrid (n = 15) embryos stained for DNA (*cyan*), microtubules (DM1-α) (*green*) and γ-tubulin (*red*). Two hybrid examples are shown to illustrate the range of hybrid phenotypes, including meiotic DNA capture and extra spindle arms (yellow arrowheads). The scale bar represents 5μm.

Bloom et al., Figure 4

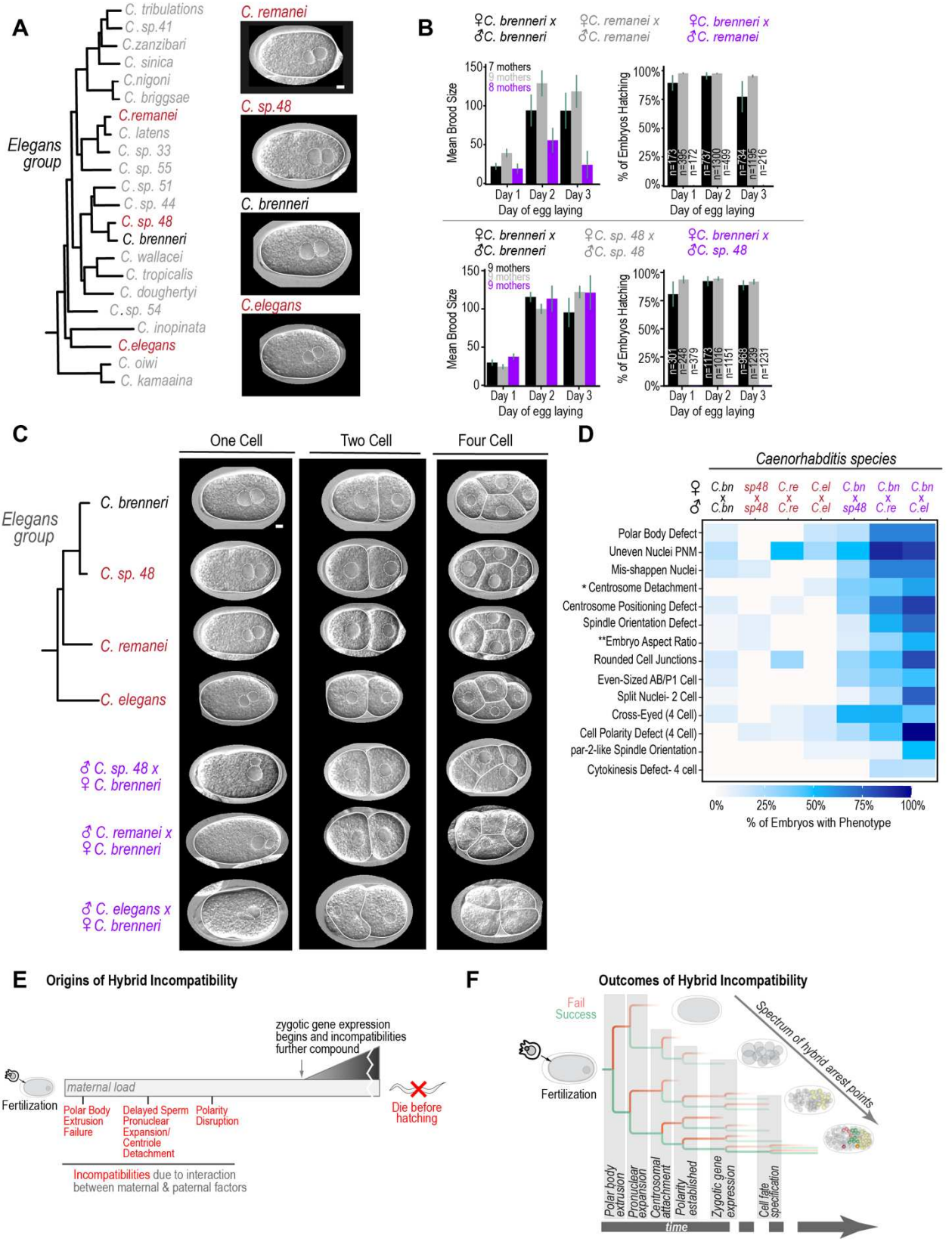

Figure 4. **A similar suite of early defects is observed in hybrid embryos generated by fertilization of *C. brenneri* oocytes with sperm from three Elegans group species. (A)** (*Left*) Phylogeny of the *Elegans* subgroup. In subsequent experiments, *C brenneri* (*black*) females were mated with males from three species *C. remanei, C. sp. 48,* and *C. elegans (indicated in red)*. (*Right*) DIC images of embryos from intraspecies crosses from each of the indicated species; embryos are shown at pronuclear meeting. (**B**) Graphs show the average brood size and % hatching for the embryos collected during the indicated days for the indicated species (*grey*, *black*) or hybrid (*purple*) cross. Day 1 is 0-24 hours post-mating; day 2 is 24-44 hours post-mating; day 3 is 44-64 hours post-mating. n refers to the number of embryos counted per cross. Error bars are ± SE. (**C**) DIC images from timelapse series of representative embryos showing them at the 1, 2, and 4-cell stages for all intraspecies (*red and black labels*) and interspecies crosses (*purple labels*). Solid white lines trace the outline of each cell, dotted white lines trace all pronuclei and nuclei. (**D**) The heatmap summarizes embryonic defects observed through the 4-cell stage for the indicated crosses; embryos were scored blinded to cross. The shading goes from no (*white*) to all (*dark blue*) of the embryos displaying the specified phenotype. (*) Centrosome positioning defects are likely under-counted (compare to centrosome tracking in *Figure 2D* and *E*) because centrosomes were tracked using only DIC images, in which it is difficult to accurately follow centrosomes without a fluorescent marker. (**) Embryo scored as displaying phenotype based on whether its aspect ratio was outside of 2 standard deviations of the average embryo aspect ratio across all wild-type embryos. (**E**) A schematic summarizing the early effects of hybrid incompatibility, prior to zygotic genome activation, and highlighting several key events that occur less reliably in hybrid embryos. (**F**) A schematic summarizing how the range of phenotypes observed in hybrid embryos may result from the fact that a number of early embryonic events become more prone to failure. Embryos in which multiple events fail sequentially exhibit more severe phenotypes and die sooner. Scale bars represent 5μm.

SUPPLEMENTAL FIGURE TITLES AND LEGENDS

Bloom et al., Figure S1

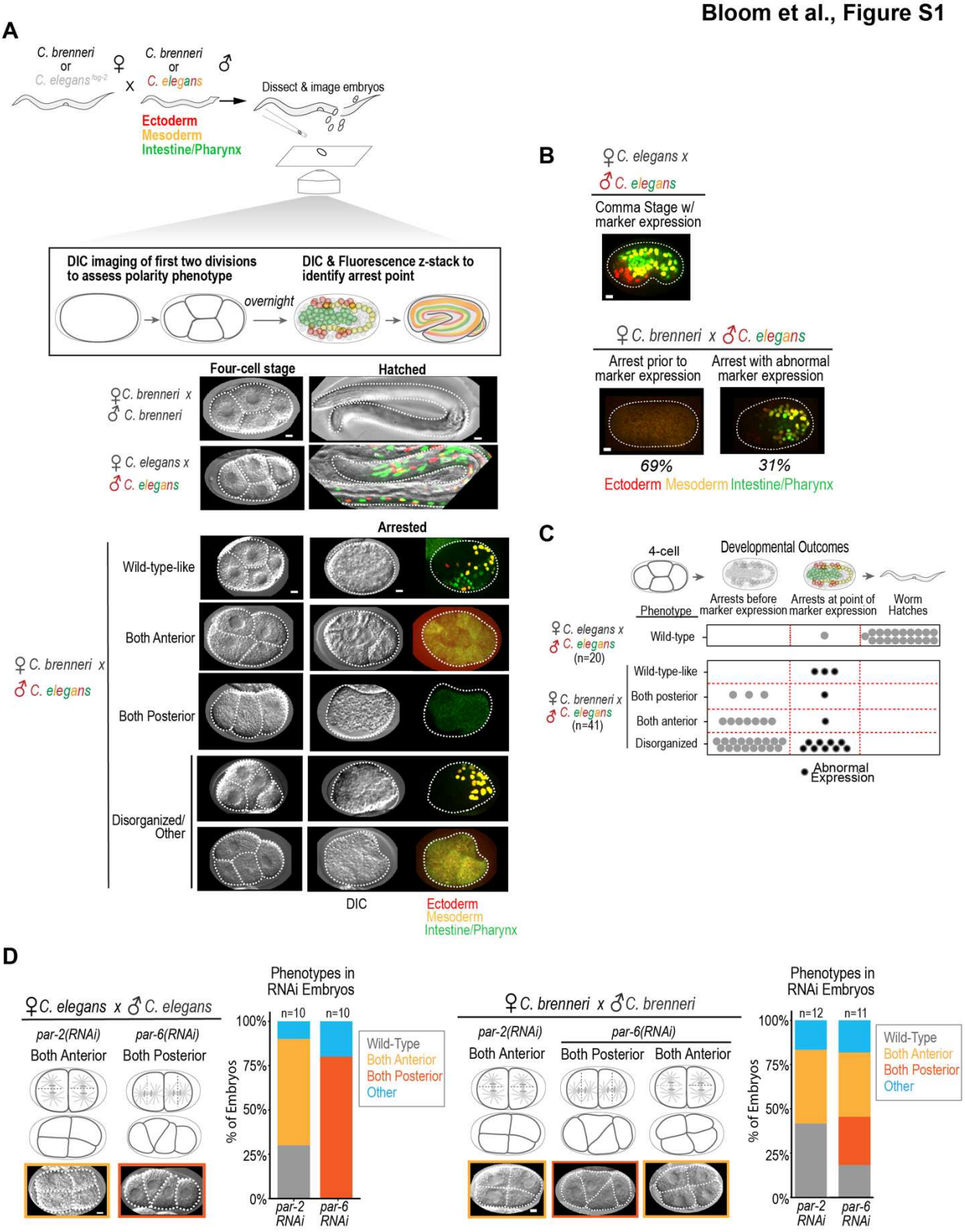

Figure S1. Polarity phenotypes at the 4-cell stage correlate with the ability of hybrid embryos to reach mid-embryogenesis and turn on tissue-specific markers. (A) The schematic illustrates the experimental workflow to detect early defects before ZGA, which occurs at the 4-cell stage, and correlate them with the ability of embryos to reach mid-embryogenesis and turn on tissue-specific markers. Briefly, *C. brenneri* or *C. elegans* (*fog-2)* females were mated to males from either *a C. elegans* strain in which the genome encodes fluorescent reporters that mark nuclei in the endoderm (*green*), mesoderm (*yellow*), and ectoderm (*red*) or *C. brenneri (unmarked)*. DIC imaging was used to film embryos through the 4-cell stage. A spinning disk confocal fluorescence z-stack was collected of the same embryos 20-24 hours later to identify the point of arrest and determine whether the tissue-specific markers had turned on. Endpoint images for larval worms are scaled to best highlight marker expression, and intensity levels are not directly comparable to the arrested hybrid embryos. **(B)** Representative maximum intensity projections of spinning disc confocal z-stacks of hybrid embryos that arrested prior to (*bottom left*) and after (*bottom right*) the onset of marker expression compared to the comma stage in control *C. elegans* intraspecies embryos (*top*). Image projections are scaled to best highlight marker expression and intensities cannot be directly compared between *C. elegans* and hybrid embryos. (**C**) Summary table displaying the results of the phenotypic analysis for the *C. elegans* and *C. brenneri* x *C. elegans* hybrid embryos. While the majority of *C.* elegans embryos (19/20) showed a wild-type 4-cell phenotype and hatched, most hybrid embryos (38/41) showed a non-wild-type-like 4-cell phenotype, and none hatched. All 3 of the hybrid embryos that exhibited a wild-type-like 4-cell orientation survived to express markers, whereas embryos exhibiting more severe polarity phenotypes rarely made it to marker expression (Both Anterior (1/4); Both Posterior (1/9)). Hybrid embryos that fell into the Disorganized/Other category had an intermediate level of success with 9/26 surviving to the point of marker expression. **(D)** DIC images of representative 4-cell stage embryos are shown for *par-2(RNAi)* and *par-6(RNAi) C. elegans* (*left*) and *C. brenneri* (*right*) embryos. The schematics highlight the 2-cell division planes giving rise to the 4-cell phenotypes, and the graphs show the phenotype frequencies for each condition. Scale bars represent 5μm.

Bloom et al., Figure S2

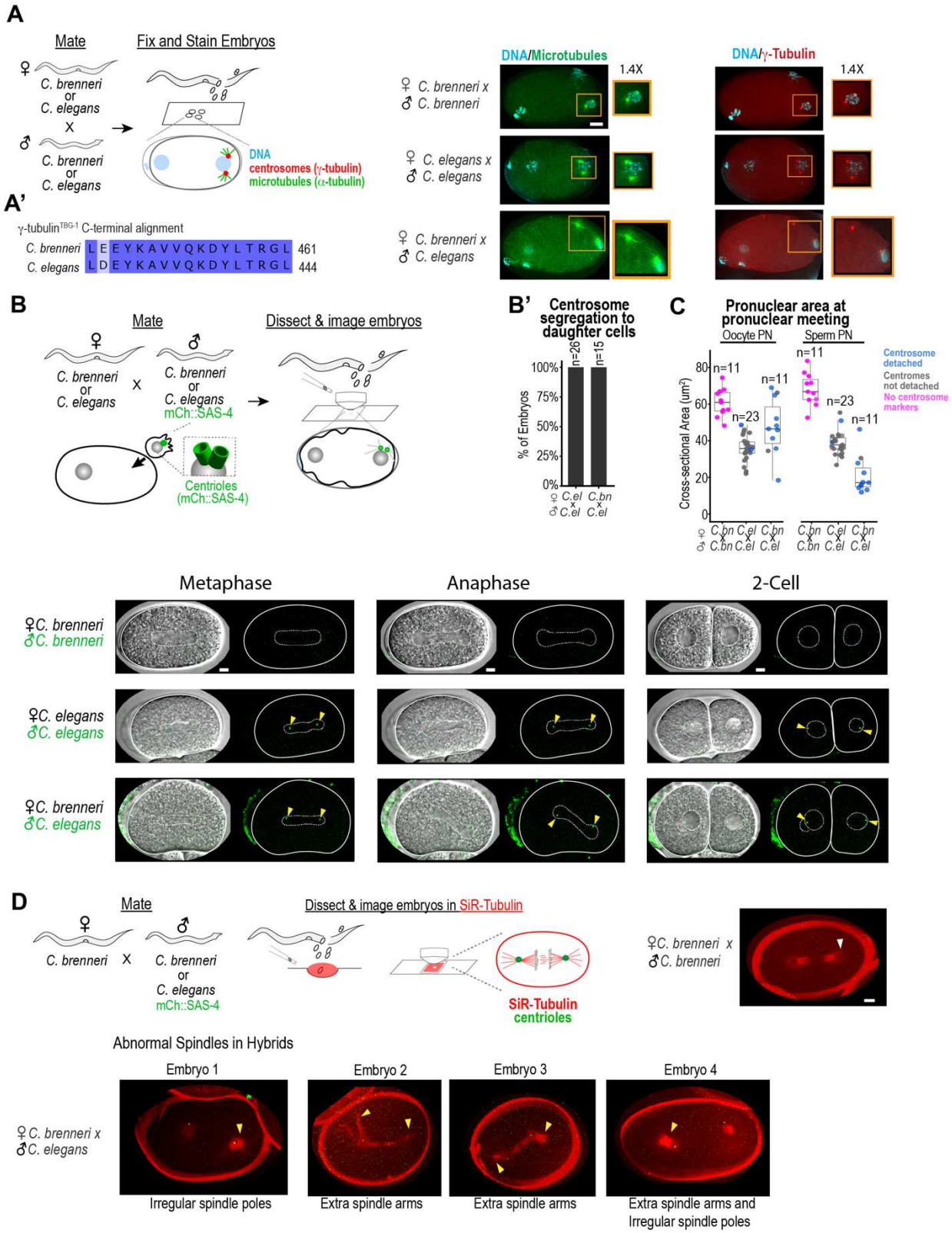

416

Figure S2. Hybrids exhibit abnormal centrosome-pronuclear attachment, polar body extrusion, male pronuclear expansion and spindle morphology (A) (*Left*) The schematic illustrates the mating regime and the predicted staining pattern of α-tubulin, γ-tubulin and DNA after the conversion of centrioles to centrosomes but prior to pronuclear migration. (*Right*) Representative images of 1-cell stage *C. brenneri* (n = 14), *C. elegans* (n=12), and hybrid (n = 12) embryos after the conversion of centrioles to centrosomes but prior to pronuclear migration, stained for DNA (*cyan*), α-tubulin (DM1-α) (*green*), and γ-tubulin (*red*). Insets are magnified 1.4X. One or both centrosomes were often detached in hybrids (11/12 embryos). Maximum intensity projections were scaled to best highlight protein localization, so intensity levels are not directly comparable across images. **(A')** Amino acid alignment of the C-terminal peptide of *C. elegans* γ-tubulin (TBG-1) against which the antibody was raised to the equivalent region of the *C. brenneri* protein. All but one residue is conserved. **(B)** (*Top*) A schematic of mating combinations of *C. brenneri* or *C. elegans* females and *C. brenneri* males or *C. elegans* males with mCherry::SAS-4 (*green*) to enable centriole tracking. (*Bottom*) Paired DIC/fluorescence overlay (*left*) and fluorescence-only (*right*) images of *C. brenneri*, *C. elegans,* and hybrid embryos at metaphase and anaphase of the first division and at the 2-cell stage. White solid lines (embryo outline) and white dotted lines (pronuclei/nuclei/spindle) are the same across DIC and fluorescence images. Yellow arrowheads mark centrioles. Images are different timepoints taken from the timelapse series of the same embryos shown in *Figure 2D & E*. Image intensities for centrioles were scaled to best show centrosome localization and cannot be directly compared across embryos. **(B')** Centriole segregation is not affected in hybrid embryos. The graph plots the percent of embryos with marked centrioles that show segregation of one sperm-derived centriole into each daughter cell (26/26 embryos in *C. elegans*; 15/15 embryos in hybrids). (**C**) The graph plots the cross-sectional area of the oocyte and sperm pronuclei at pronuclear meeting for the indicated crosses. Centriole detachment is indicated by blue circles and wild-type-like centriole separation by the gray circles. In *C. brenneri*, centrioles were not labeled and detachment was not scored (*pink circles*). Median (IQR) for female pronuclear cross-sectional area is 61 (51-71), 36 (30-42), 46 (26-66) μm^2 for *C. brenneri, C. elegans*, and hybrid embryos, respectively. Median (IQR) for male pronuclear cross-sectional area is 67 (56-78), 38 (32-44), 17 (7-27) μm^2 for *C. brenneri, C. elegans*, and hybrid embryos, respectively. (**D**) The schematic (*top, left*) illustrates how *C. brenneri* females were mated with *C. brenneri* males as a control or with *C. elegans* males with mCherry::SAS-4-marked centrioles to enable live tracking of centrioles (*green*), and how embryos were dissected into the vital dye SiR-Tubulin (*red*) to monitor microtubules. Images show maximum intensity projections that capture SiR-Tubulin-stained spindles in a *C. brenneri* embryo (*top, right)* and four examples of hybrid embryos (*bottom*) at anaphase. The white arrowhead indicates normal spindle morphology, whereas yellow arrowheads point to spindle poles or extra spindle arms in hybrid embryos. Embryos categorized as having abnormal spindles in the graph in *Figure 3D* displayed phenotypes similar to the ones shown here. Intensities were scaled to best show SiR-Tubulin signal and cannot be compared across embryos. Maximum intensity projections were made to include slices containing centrioles. Centriole intensities are scaled the same across images. *C. brenneri* embryos do not contain marked centrioles. Scale bars represent 5μm.

Bloom et al., Figure S3

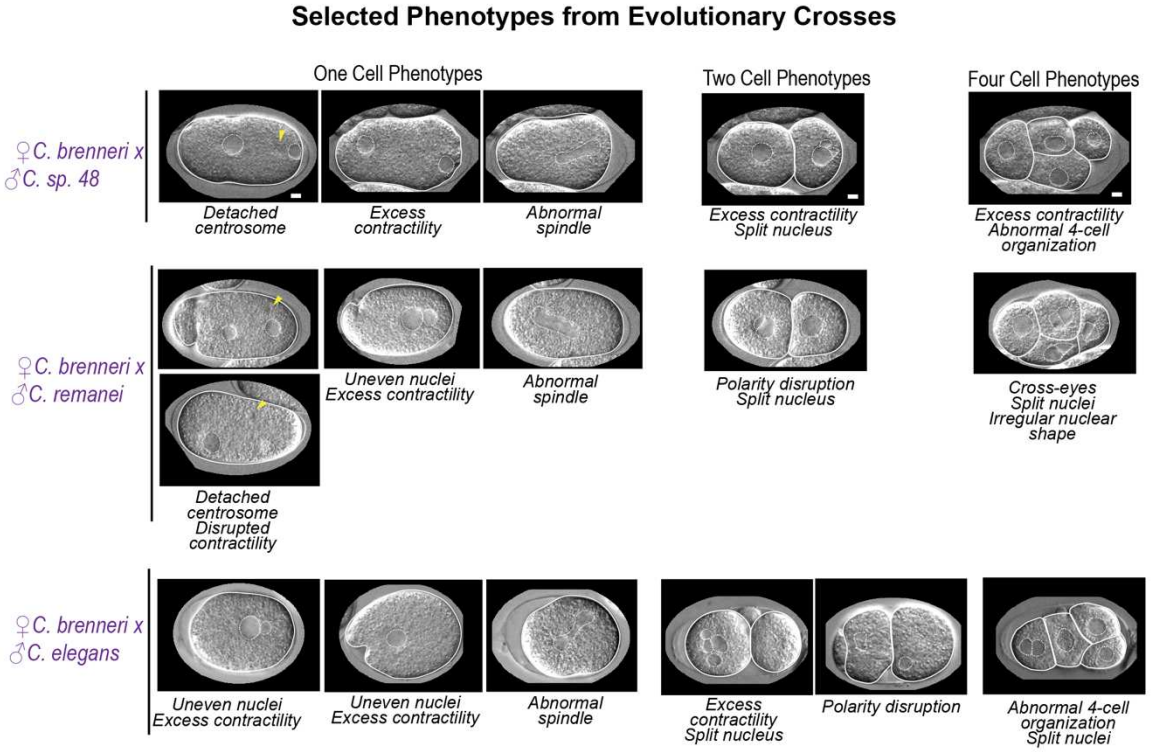

Figure S3. Gallery of hybrid phenotypes. Gallery of 1, 2, 4-cell hybrid embryos from *C. brenneri* females crossed with males from *C. sp. 48* (*top*), *C. remanei* (*middle*), and *C. elegans* (*fog-2(q71)*) (*bottom*). Embryos were dissected and monitored by DIC through the first two cell divisions. Embryos were blind-scored for phenotypes in time-lapse images. The gallery highlights abnormal phenotypes found in 1 to 4-cell embryos. White solid lines outline the embryo and white dotted lines outline the pronuclei, spindle, and nuclei. Yellow arrowheads highlight detached centrosomes. The scale bar represents 5μm.

Video S1. Similar phenotypes are observed after RNAi of *par-2* and *par-6* in *C. elegans* and *C. brenneri* (related to Figure 1D-E). Timelapse sequences of C. brenneri (*top row*) and *C. elegans* embryos (*bottom row*). Control embryos are shown on the left, *par-2(RNAi)* embryos in the middle and *par-6(RNAi)* embryos on the right. Still images of the *C. brenneri par-6(RNAi)* and *par-2(RNAi)* embryos shown here are also shown in *Figure 1E*. Cleavage sites in the *par-2(RNAi)* (*yellow arrows*) and *par-6(RNAi)* (*orange arrows*) embryos are indicated. 26 x 1um z-stacks were collected every 30 seconds and movies were created by compiling the best z-slice from the z-stack collected at each timepoint. Playback frame rate is 5 frames/s.

Video S2. The sperm pronucleus remains small leading to centrosome detachment in hybrids of *C. brenneri* females and *C. elegans* males (related to Figure 2C-F and Figure S2B,B'). Representative timelapse sequences showing centriole position and nuclear size during the first cell division in a *C. elegans* embryo (*top row*) and a *C. brenneri* x *C. elegans* hybrid (*bottom row*). Still images of the wild-type and hybrid embryos shown are also included in *Figure 1D,E* and *Figure S2B,B'*. Yellow arrows point to the centrosomes. Black dotted lines trace the outline of the pronuclei. Movies are composed of a single z DIC slice overlaid with fluorescence maximum intensity projections of 19 x 1.5 μm z-stacks acquired every 30 seconds. Intensity values for centrioles were scaled to best highlight centrosome positioning are not comparable between different embryos. Playback rate is 5 frames/s.

Video S3. Aberrant spindle morphologies are observed in hybrid embryos of *C. brenneri* females and *C. elegans* males (related to Figure 3C,D and Figure S2D). Representative timelapse sequences showing centrioles (*green*) and microtubules (*red*) in reference *C. brenneri* (first column) and *C. elegans* (second column) embryos along with two *C. brenneri* x *C. elegans* hybrids. Sequences run from ooctye pronuclear appearance through the first cell division. Still images of the embryos shown are also included in *Figure 3C*. The centrioles (*yellow arrows*), aberrant spindle morphology (*cyan arrows*), and meiotic spindle capture (*dark blue arrows*) are indicated. A 27 x 1 μm z-stack was collected every minute, and movies are composed of maximum intensity projections of the subset of z-planes that best show centrosomes and spindles for each timepoint. Intensity values for spindles are not comparable between different embryos because of the variable amount of dye that may enter the embryo. Playback speed is 5 frames/s.

Video S4. A similar suite of early defects is observed in hybrids between *C. brenneri* females and males from three Elegans group species (related to Figure 4C,D, Figure 1D,E, Figure S1C,E and Figure S3). Representative timelapse sequences of the early embryonic cell divisions in wild-type *C. brenneri*, *C. sp. 48*, *C. remanei* and *C. elegans* embryos (top row) along with their hybrids (*bottom row*). Still images of embryos shown are also included in *Figure 4C*, *Figure S1A* (*Disorganized/other)* and *Figure S3*. Black dotted lines trace pronuclei. Movies are composed of single z slices chosen from 26 x 1 μm z-stacks acquired every 30sec. Playback rate is 5 frames/s.

Table S1. Description of manual scoring data and measured features to Figures 3 and 4 and STAR Methods. In the All Scored Embryos tab, each cross type is highlighted in a different color. In the Considered Phenotypes tab, rows highlighted in yellow consistently showed a phenotype during embryo scoring.

STAR METHODS

RESOURCE AVAILABILITY

Lead contact

Further information and requests for resources and reagents should be directed to and will be fulfilled by the lead contact, Scott Rifkin ([31,32]).

Materials availability

All strains and other reagents generated in this study are freely available from the lead contact upon request. *C. brenneri, C. remanei,* and *C. elegans* (*fog-2*) strains can be obtained from the Caenorhabditis Genetics Center (CGC). *C. sp. 48* was a gift from M.-A. Félix.

Data and Code Availability

- The custom computer code generated for this project is publicly available through https://gitlab.com/evodevosyslabpubs/Bloom_etal_2025 and will be deposited at Zenodo
- Any additional information required to reanalyze the data reported in this paper will be available from the lead contact upon request

EXPERIMENTAL MODEL AND STUDY PARTICIPANT DETAILS

C. elegans, C. brenneri, C. sp. 48, and *C. remanei* strains were maintained at 20°C on standard Nematode Growth Media (NGM) plates seeded with OP50 bacteria. The genotypes of the *C. elegans* strains used in this study are described in Reagents and Resources.

METHOD DETAILS

Strains

C. brenneri was always LKC28; *C. sp. 48* was always BRC20359; *C. remanei* was always EM464, and *C. elegans* females were always JK574, which has a *fog-2* mutation that makes hermaphrodites females.

Mating

For all crosses, L4-stage females were placed with males on a 35mm plate seeded with OP50 and left overnight at 20C for mating; females were dissected the following day. A 1:2 ratio of females to males was used for all crosses except for interspecies crosses with *C. elegans* males, for which a 1:3 ratio was used because C*. elegans* males are worse at mating than dioecious males.[58,59]

Dissections

Gravid females were dissected in Boyd Buffer (59.9 mM $NaCl_2$, 32.2 mM KCl, 2.8 mM Na_2HPO4, 1.8 mM $CaCl_2$, 5mM HEPES pH 7.2, 0.2% glucose, 2.1 mM $MgCl_2$;)[43,60] and were transferred by mouth pipette to a 2% agarose pad made in Boyd Buffer for imaging. An 18x18mm coverslip was placed over the pad and the edges of the coverslip were sealed with VALAP (1:1:1 Vaseline, Lanolin, and Parafin) to prevent drying out. We compared five different osmotic support buffers (meiosis media, Boyd buffer, 0.5X Egg Salts, 0.7X Egg Salts, and 1X Egg Salts)[43,60–62] but no rescue of early arrest phenotypes was observed for any of them.

Brood size & embryonic viability measurements

To measure the number of embryos laid and assess their viability (defined hatching), individual L4 females were placed on a 35 mm NGM plate seeded with OP50 along with 2 or 3 males (see Mating section) and left to mate overnight at 20°C. After 24 hours, the males were removed and the females were moved to a second 35mm plate. Females were transferred again to a third 35 mm plate 20 hours later (44 hours after the start of mating). After 64 hours, the females were removed from the third plate. After each transfer, the number of freshly laid embryos on the plate from which the female was removed was counted and the plate was returned to 20°C. Since viable embryos hatch within 20 hours of being laid we waited 20-24 hours after first count was made and then counted the number of hatched and unhatched embryos to measure viability.

RNA production

The *C. brenneri* orthologs of the *C. elegans par-2* and *par-6* genes were identified based on annotation in WormBase; ortholog identity was confirmed using reciprocal BLAST. DNA templates for generating dsRNAs were generated by PCR using primers designed using Primer3 (https://primer3.ut.ee/) to amplify a 400-800 bp region of each gene from genomic DNA (see KEY RESOURES Table for sequences). Primers contained T3 or T7 promoters to enable transcription reactions. Primers for dsRNAs targeting the *C. elegans* genes were the same as those employed in a prior RNAi-based screen.[49] PCR reactions were cleaned and used as templates in T3 and T7 transcription reactions. T3 and T7 RNA products were mixed at equimolar amounts, cleaned, and annealed by adding 3X Soaking buffer (32.7 mM Na_2HPO_4, 16.5 mM KH_2PO_4, 6.3 mM NaCl, 14.1 mM NH_4Cl) to a final concentration of 1X and incubating reactions at 68C for 10 minutes then 37°C for 30 minutes.

RNA interference

For *C. elegans*, larval (L4 stage) female (JK574) worms were injected with dsRNA in the body cavity and left to recover at 20°C for 4 hours before singling and mating with male *C. elegans* (JK574) worms at 20°C overnight before imaging. For *C. brenneri*, larval (L4 stage) females (LKC28) were mated to male *C. brenneri* (LKC28) worms on a 35mm OP50 plate overnight at 20°C. Gravid females were injected with

dsRNA in both gonad arms, left to recover for 3 hours (20°C), before singling and leaving overnight at 20°C for 22 hours before imaging.

Imaging and analysis of early and late embryogenesis

After mating, dissection, and mounting as described above, we monitored early embryogenesis using differential interference contrast (DIC) optics to acquire 26 x 1µm z-stacks at 30-45 second intervals. In most experiments, embryos were imaged through the four-cell stage. Images were acquired using either an inverted Zeiss Axio Observer Z1 system equipped with a Yokogawa CSU-X1 spinning-disk, 63X 1.40 NA Plan Apochromat lens (Zeiss), and a QuantEm: 512SC camera (Teledyne Photometrics), or on a Nikon Ti2 microscope equipped with a Yokogawa CSU-X1 spinning disk, a 60X, 1.4 NA PlanApochromat lens, and an iXon Life EMCCD camera. For monitoring fluorescent marker turn-on, embryos that had been filmed by DIC during early embryogenesis were allowed to develop for 20 additional hours at 20°C before the acquisition of 26 x 1µm z-stack using confocal fluorescence microscopy (488 and 561 nm lasers) and DIC optics. For all measurements, embryos were cropped from time-lapse series and measurements were made using FIJI.[63] Table S1 has descriptions of the features scored or measured.

Centriole Positioning in Early Hybrid Embryos

C. elegans (OD3701) or *C. brenneri* (LKC28) males were crossed to *C. brenneri* (LKC28) or *C. elegans* (JK574) females and left to mate overnight at 20°C for 24 hours. Female worms were dissected and embryos mounted as described above. Embryos were imaged by collecting 19 x 1.5 µm z-stacks every 30 sec, capturing DIC and fluorescence (561nm laser at 15% power, 2x2 binning, 100ms exposure) through the two-cell stage. FIJI was used to crop and rotate images for scoring. Centrioles were considered detached when centrioles were > 9µm apart. FIJI was used to create maximum projections and to scale images for figures. The image intensities were scaled to best visualize centrosome position within the early embryo.

Spindle Angle, Pronuclear Localization and Size, and Embryo Aspect Ratio Analysis

Embryos were cropped from timelapse series and measurements were made using FIJI. P0 spindle angle was measured relative to the long axis of the embryo; the angle was assessed from metaphase onset through the following 3.5-4.5 minutes. Images were converted to maximum intensity projections, since centrioles were in different z-planes for part of the first cell division, and then each embryo was scored for centrosome detachment before pronuclear meeting or centrosome mis-localization at pronuclear meeting. Sperm pronucleus length and width was measured at the appearance of the oocyte-derived pronucleus, and sperm-derived pronuclear area was then calculated by using the equation for the area of an ellipse : $\pi \frac{length}{2} \frac{width}{2}$. Embryo aspect ratio was calculated as the ratio of cross-sectional width to cross-sectional length of P0 embryos.

Centriole Positioning and Microtubule tracking

C. brenneri (LKC28) females were crossed with *C. brenneri* (LKC28) males or *C. elegans* (OD3701) males, and *C. elegans* (JK574) females were crossed with *C. elegans* (OD3701) males. Female worms were dissected into 250 nM SiR-Tubulin dye (Cytoskeleton, cat# CY-SC002). To generate an agar pad containing SiR-Tubulin, 15µL of 5µM dye was added on top of a 2% agarose pad made in Boyd Buffer. One-cell embryos were transferred by mouth pipette, covered with an 22x22mm coverslip, and sealed

with VALAP before imaging. Embryos were imaged on a Nikon Ti2 microscope equipped with a Yokogawa CSU-X1 (Nikon) spinning disk, a 60X, 1.4 NA PlanApochromat lens, and an iXon Life EMCCD camera. A 27 x 1 µm z-stack was collected every min, capturing DIC and fluorescence (561nm at 15% power, 2x2 binning, 100ms exposure, and 640nm at 40% power and 200ms exposure) through the two-cell stage. Images were cropped and rotated for analysis using FIJI. Timelapse SiR-Tubulin sequences were created by generating maximum intensity projections of the subset of the best subset of 14 z-slices containing the spindle and were scaled to show the best signal unobscured by the SiR-Tubulin coating the eggshell. Image intensities were scaled independently for each embryo because dye uptake varies between embryos. Centriole channel images were created using maximum projections to best capture the centrioles.

Developmental Imaging

For the arrest point experiment in Fig. S1B, *C. elegans* males (OD 1719)[30] or *C. brenneri* males (LKC28) were mated with *C. elegans* females (JK574) or *C. brenneri* females (LKC28) for 24hrs at 20°C. OD1719 animals express germ-layer markers: ectoderm (Pdlg-1::mCherry::his-72 and Pcnd-1::mCherry::his-72), endoderm (Ppha-4::pha-4::GFP), and mesoderm (Phlh-1::his-72::mCherry and Phlh-1::his-72::GFP). For this experiment, embryogenesis was captured by dissecting females in Boyd Buffer and transferring the embryos to a 384-well imaging plate containing 70uL Boyd Buffer. Embryos were imaged over a 10-hour time-course as previously described.[30]

Immunofluorescence of Early Embryos

Slides for immunofluorescence were generated by dipping in subbing solution prepared by dissolving 0.1g gelatin in 25 mL of distilled water heated to 60°C, cooling to 40°C, adding 0.01g chromalum, and 15mg poly-lysine HBr. Subbing solution was left to stir at 40°C for 2 hours before sterile filtering and storage at 4°C. Slides were dipped in subbing solution heated to 50°C and allowed to dry for 6 hours. 20-30 mated female animals were placed in a 4µl drop of distilled water placed in the center of the slide and an 18x18 coverslip was placed on top. Worms were compressed by pushing on the coverslip with a pipet tip, embryos were pushed out of the mothers, and slides were plunged into liquid nitrogen. Slides were retrieved and a razor blade was used to pop the coverslips off each slide. Slides were immediately immersed in -20°C cold methanol for a 15-minute fixation. Samples were fixed and stained as previously described.[64] For detection of PAR-2, slides were incubated in unconjugated primary antibody (Mouse-anti-PAR-2 1:1000 dilution) overnight at 4°C, washed, and then incubated with fluorescent secondary antibody (Donkey-anti-Mouse-Cy5) for 30min at room temperature. To stain for centrosomes and microtubules, embryos were incubated with directly-labeled α-tubulin antibodies (DM1-α-FITC 1:1000 dilution; Sigma Aldrich F2168) and anti-γ-tubulin-CY3 (C-terminal antigen: LDEYKAVVQKDYLTRGL; 1:300 dilution)[45] for 60 minutes at room temperature. Slides were washed with PBST buffer, and 1 µg/ml Hoechst was added during the last 10-minute wash. Two final washes were performed and 15 µl of ProLong Glass Antifade Mount (ThermoFisher) mounting and curing solution was added before covering the embryos with an 18 x 18mm coverslip. The slides were left to cure at room temperature for 24 hours in a dark chamber. Samples were imaged on a DeltaVision (GE Healthcare) epifluorescence scope equipped with a 100X 1.4NA oil immersion objective. Images were deconvolved using SoftWoRx software (Cytvia). Maximum projections were made using FIJI and image intensities adjusted for best visualization of signal.

Evolutionary analysis of hybrid embryos

664 *C. brenneri* females were mated to males of *C. sp. 48* and*C. remanei* in a ratio of 1:2 and to males of *C*
665 *elegans* in a ratio of 1:3 on individual mating plates. Plates were left overnight at 20°C for mating as
666 described above. Twenty-four hours later, embryos were dissected from gravid female animals in Boyd
667 buffer and mounted as described above. DIC images of early embryogenesis were acquired as described
668 above collecting images every 30s until the 4-cell stage or later. Embryos were cropped and rotated for
669 further analysis. Image names were anonymized by JB, and embryos scored by RG as either a 1 (display
670 phenotype) or 0 (do not display phenotype) for the phenotypes listed in Table S1.

671

672 **Divergence time estimates**

673 We downloaded complete *Caenorhabditis* genomes from https://caenorhabditis.org, extracted the
674 longest isoforms for each protein, and used the species tree estimated by Orthofinder. Branch lengths of
675 the estimated species tree represent molecular phylogenetic distance along the branch.[65] We used these
676 branch lengths to determine the relative divergence of protein coding sequences between *C. brenneri*
677 and the three other species.

678

679 **Quantification and Statistical Analysis**

680 All graphs shown in the manuscript were created and analyzed in R (Rstudio).[66]

681

682 **REFERENCES:**
683
684 1. Coyne, J. A. & Orr, H. A. Patterns of reproductive isolation in Drosophila. *Evolution* **43**, 362–381
685 (1989).
686 2. Dobzhansky, T. *Genetics and the Origin of Species, By Theodosius Dobzhansky*. (1937).
687 3. Mayr, E. *Animal Species and Evolution*. (Harvard University Press, 1963).
688 4. Mayr, E. *Populations, Species, and Evolution: An Abridgment of Animal Species and Evolution*. vol.
689 19 (Harvard University Press, 1970).
690 5. Sawamura, K., Taira, T. & Watanabe, T. K. Hybrid lethal systems in the Drosophila melanogaster
691 species complex. I. The maternal hybrid rescue (mhr) gene of Drosophila simulans. *Genetics* **133**,
692 299–305 (1993).
693 6. Sawamura, K., Yamamoto, M. T. & Watanabe, T. K. Hybrid lethal systems in the Drosophila
694 melanogaster species complex. II. The Zygotic hybrid rescue (Zhr) gene of D. melanogaster.
695 *Genetics* **133**, 307–313 (1993).
696 7. Forejt, J. Hybrid sterility in the mouse. *Trends in Genetics* **12**, 412–417 (1996).
697 8. Mihola, O., Trachtulec, Z., Vlcek, C., Schimenti, J. C. & Forejt, J. A Mouse Speciation Gene
698 Encodes a Meiotic Histone H3 methyltransferase. *Science* **323**, 373–5 (2009).
699 9. Barbash, D. A., Siino, D. F., Tarone, A. M. & Roote, J. A rapidly evolving MYB-related protein
700 causes species isolation in Drosophila. *Proceedings of the National Academy of Sciences of the*
701 *United States of America* **100**, 5302–5307 (2003).
702 10. Barbash, D. A., Awadalla, P. & Tarone, A. M. Functional divergence caused by ancient positive
703 selection of a Drosophila hybrid incompatibility locus. *PLoS Biology* **2**, 839–848 (2004).
704 11. Sawamura, K. & Yamamoto, M.-T. Characterization of a reproductive isolation gene, zygotic hybrid
705 rescue, of Drosophila melanogaster by using minichromosomes. *Heredity* **79**, 97–103 (1997).
706 12. Barbash, D. A. Ninety years of Drosophila melanogaster hybrids. *Genetics* **186**, 1–8 (2010).
707 13. Wittkopp, P. J., Haerum, B. K. & Clark, A. G. Evolutionary changes in cis and trans gene regulation.
708 *Nature* **430**, 85–88 (2004).

14. Coolon, J. D., McManus, C. J., Stevenson, K. R., Graveley, B. R. & Wittkopp, P. J. Tempo and mode of regulatory evolution in Drosophila. *Genome Research* **24**, 797–808 (2014).
15. Bundus, J. D., Wang, D. & Cutter, A. D. Genetic basis to hybrid inviability is more complex than hybrid male sterility in Caenorhabditis nematodes. *Heredity* **121**, 169–182 (2018).
16. Bundus, J. D., Alaei, R. & Cutter, A. D. Gametic selection, developmental trajectories, and extrinsic heterogeneity in Haldane's rule. *Evolution* **69**, 2005–2017 (2015).
17. Dey, A., Jin, Q., Chen, Y. C. & Cutter, A. D. Gonad morphogenesis defects drive hybrid male sterility in asymmetric hybrid breakdown of Caenorhabditis nematodes. *Evolution and Development* **16**, 362–372 (2014).
18. Bi, Y. *et al.* A Genome-Wide Hybrid Incompatibility Landscape between Caenorhabditis briggsae and C. nigoni. *PLoS Genetics* **11**, 1–26 (2015).
19. Baugh, L. R., Hill, A. A., Slonim, D. K., Brown, E. L. & Hunter, C. P. Composition and dynamics of the *Caenorhabditis elegans* early embryonic transcriptome. *Development* **130**, 889–900 (2003).
20. Guven-Ozkan, T., Nishi, Y., Robertson, S. M. & Lin, R. Global Transcriptional Repression in C. elegans Germline Precursors by Regulated Sequestration of TAF-4. *Cell* **135**, 149–160 (2008).
21. Stoeckius, M., Grün, D. & Rajewsky, N. Paternal RNA contributions in the Caenorhabditis elegans zygote. *The EMBO Journal* **33**, 1740–1750 (2014).
22. Macchietto, M. *et al.* Comparative Transcriptomics of Steinernema and Caenorhabditis Single Embryos Reveals Orthologous Gene Expression Convergence during Late Embryogenesis. *Genome Biology and Evolution* **9**, 2681–2696 (2017).
23. Cowan, C. R. & Hyman, A. A. Centrosomes direct cell polarity independently of microtubule assembly in C. elegans embryos. *Nature* **431**, 92–96 (2004).
24. Rose, L. & Gonczy, P. Polarity establishment, asymmetric division and segregation of fate determinants in early C. elegans embryos. *WormBook* 1–43 (2014) doi:10.1895/wormbook.1.30.2.
25. Baird, S. E. & Yen, W. C. Reproductive isolation in Caenorhabditis: Terminal phenotypes of hybrid embryos. *Evolution and Development* (2000) doi:10.1046/j.1525-142X.2000.00031.x.

26. Baird, S. E. & Seibert, S. R. Reproductive isolation in the Elegans-Group of Caenorhabditis. **5**, 18–25 (2013).

27. Rockman, M. V. *et al.* A phylogeny and molecular barcodes for Caenorhabditis, with numerous new species from rotting fruits. *BMC Evolutionary Biology* **11**, 339 (2011).

28. Cutter, A. D., Garrett, R. H., Mark, S., Wang, W. & Sun, L. Molecular evolution across developmental time reveals rapid divergence in early embryogenesis. 359–373 (2019) doi:10.1002/evl3.122.

29. Landry, C. R. *et al.* Compensatory cis-trans Evolution and the Dysregulation of Gene Expression in Interspecific Hybrids of Drosophila. **1822**, 1813–1822 (2005).

30. Wang, S. *et al.* A high-content imaging approach to profile *C. elegans* embryonic development. *Development* dev.174029 (2019) doi:10.1242/dev.174029.

31. Green, R. A. *et al.* Automated profiling of gene function during embryonic development. *Cell* **187**, 3141-3160.e23 (2024).

32. Memar, N. *et al.* Twenty million years of evolution: The embryogenesis of four Caenorhabditis species are indistinguishable despite extensive genome divergence. *Developmental Biology* 1–18 (2018) doi:10.1016/j.ydbio.2018.12.022.

33. Levin, M., Hashimshony, T., Wagner, F. & Yanai, I. Developmental Milestones Punctuate Gene Expression in the Caenorhabditis Embryo. *Developmental Cell* **22**, 1101–1108 (2012).

34. Boveri, T. Zellenstudien II: Die Befruchtung und Teilung des Eies von Ascaris megalocephala. *Jenaer Zeitschrift für Naturwissenschaft* 685–882, plates XIX-XXIII (1888).

35. Albertson, D. G. Formation of the first cleavage spindle in nematode embryos. *Developmental Biology* **101**, 61–72 (1984).

36. Oegema, K. Cell division. *WormBook* (2006) doi:10.1895/wormbook.1.72.1.

37. McNally, K. L. P. *et al.* Kinesin-1 Prevents Capture of the Oocyte Meiotic Spindle by the Sperm Aster. *Developmental Cell* **22**, 788–798 (2012).

38. Severson, A. F., Von Dassow, G. & Bowerman, B. Oocyte Meiotic Spindle Assembly and Function. in *Current Topics in Developmental Biology* vol. 116 65–98 (Elsevier, 2016).

39. Cuenca, A. A., Schetter, A., Aceto, D., Kemphues, K. & Seydoux, G. Polarization of the C. elegans zygote proceeds via distinct establishment and maintenance phases. *Development* **130**, 1255–1265 (2003).

40. Munro, E., Nance, J. & Priess, J. R. Cortical Flows Powered by Asymmetrical Contraction Transport PAR Proteins to Establish and Maintain Anterior-Posterior Polarity in the Early C. elegans Embryo. *Developmental Cell* **7**, 413–424 (2004).

41. Bienkowska, D. & Cowan, C. R. Centrosomes Can Initiate a Polarity Axis from Any Position within One-Cell C. elegans Embryos. *Current Biology* **22**, 583–589 (2012).

42. Hoege, C. & Hyman, A. A. Principles of PAR polarity in Caenorhabditis elegans embryos. *Nat Rev Mol Cell Biol* **14**, 315–322 (2013).

43. Boyd, L., Guo, S., Levitan, D., Stinchcomb, D. T. & Kemphues, K. J. PAR-2 is asymmetrically distributed and promotes association of P granules and PAR-1 with the cortex in *C. elegans* embryos. *Development* **122**, 3075–3084 (1996).

44. Hoege, C. *et al.* LGL Can Partition the Cortex of One-Cell Caenorhabditis elegans Embryos into Two Domains. *Current Biology* **20**, 1296–1303 (2010).

45. Hannak, E., Kirkham, M., Hyman, A. A. & Oegema, K. Aurora-A kinase is required for centrosome maturation in *Caenorhabditis elegans*. *The Journal of Cell Biology* **155**, 1109–1116 (2001).

46. Hamill, D. R., Severson, A. F., Carter, J. C. & Bowerman, B. Centrosome Maturation and Mitotic Spindle Assembly in C. elegans Require SPD-5, a Protein with Multiple Coiled-Coil Domains. *Developmental Cell* **3**, 673–684 (2002).

47. Hannak, E. *et al.* The kinetically dominant assembly pathway for centrosomal asters in *Caenorhabditis elegans* is γ-tubulin dependent. *The Journal of Cell Biology* **157**, 591–602 (2002).

48. Ohta, M. *et al.* Polo-like kinase 1 independently controls microtubule-nucleating capacity and size of the centrosome. *Journal of Cell Biology* **220**, e202009083 (2021).

786 49. Sönnichsen, B. *et al.* Full-genome RNAi profiling of early embryogenesis in Caenorhabditis
787 elegans. *Nature* **434**, 462–469 (2005).
788 50. Grill, S. W., Gönczy, P., Stelzer, E. H. K. & Hyman, A. A. Polarity controls forces governing
789 asymmetric spindle positioning in the Caenorhabditis elegans embryo. *Nature* **409**, 630–633
790 (2001).
791 51. Malone, C. J. *et al.* The C. elegans Hook Protein, ZYG-12, Mediates the Essential Attachment
792 between the Centrosome and Nucleus. *Cell* **115**, 825–836 (2003).
793 52. Minn, I., Rolls, M. M., Hanna-Rose, W. & Malone, C. J. SUN-1 and ZYG-12, Mediators of
794 Centrosome–Nucleus Attachment, Are a Functional SUN/KASH Pair in Caenorhabditis elegans.
795 *MBoC* **20**, 4586–4595 (2009).
796 53. Gönczy, P., Pichler, S., Kirkham, M. & Hyman, A. A. Cytoplasmic Dynein Is Required for Distinct
797 Aspects of Mtoc Positioning, Including Centrosome Separation, in the One Cell Stage
798 *Caenorhabditis elegans* Embryo. *The Journal of Cell Biology* **147**, 135–150 (1999).
799 54. Meyerzon, M. *et al.* Centrosome attachment to the C. elegans male pronucleus is dependent on the
800 surface area of the nuclear envelope. *Developmental Biology* **327**, 433–446 (2009).
801 55. Cheng, N. N., Kirby, C. M. & Kemphues, K. J. Control of Cleavage Spindle Orientation in
802 Caenorhabditis elegans: The Role of the Genes par-2 and par-3.
803 56. McNally, K. L. & McNally, F. J. Fertilization initiates the transition from anaphase I to metaphase II
804 during female meiosis in C. elegans. *Developmental Biology* **282**, 218–230 (2005).
805 57. Cutter, A. D. Divergence Times in Caenorhabditis and Drosophila Inferred from Direct Estimates of
806 the Neutral Mutation Rate. *Molecular Biology and Evolution* **25**, 778–786 (2008).
807 58. Anderson, J. L., Morran, L. T. & Phillips, P. C. Outcrossing and the Maintenance of Males within C.
808 elegans Populations. *Journal of Heredity* **101**, S62–S74 (2010).
809 59. Ebert, M. S. Evolution remodels olfactory and mating-receptive behaviors in the transition from
810 female to hermaphrodite reproduction. *OPEN ACCESS*.

60. Bao, Z. & Murray, J. I. Mounting *Caenorhabditis elegans* Embryos for Live Imaging of Embryogenesis: Figure 1. *Cold Spring Harb Protoc* **2011**, pdb.prot065599 (2011).
61. Tagawa, A., Rappleye, C. A. & Aroian, R. V. pod-2, along with pod-1, Defines a New Class of Genes Required for Polarity in the Early Caenorhabditis elegans Embryo. *Developmental Biology* **233**, 412–424 (2001).
62. Edgar, L. G. Chapter 13 Blastomere Culture and Analysis. in *Methods in Cell Biology* vol. 48 303–321 (Elsevier, 1995).
63. Schindelin, J. *et al.* Fiji: an open-source platform for biological-image analysis. *Nat Methods* **9**, 676–682 (2012).
64. Oegema, K., Desai, A., Rybina, S., Kirkham, M. & Hyman, A. A. Functional Analysis of Kinetochore Assembly in *Caenorhabditis elegans*. *The Journal of Cell Biology* **153**, 1209–1226 (2001).
65. Emms, D. M. & Kelly, S. OrthoFinder: phylogenetic orthology inference for comparative genomics. *Genome Biol* **20**, 238 (2019).
66. R Core Team. R: A Language and Environment for Statistical Computing. R Foundation for Statistical Computing (2023).

828 KEY RESOURCES TABLE

829

REAGENT or RESOURCE	SOURCE	IDENTIFIER
Antibodies		
Mouse-anti-PAR-2	Hoege et. al., 2010 PMID: 20579886	
DM1-alpha-FITC	Sigma Aldrich	F2168
γ-tubulin-Cy3	Hannak et al., 2001 PMID: 11748251	
SPD-5-Cy5	Dammerman et al., 2004 PMID: 15572125	
Donkey-anti-Rabbit-Cy5	Jackson ImmunoResearch	711-175-152
Bacterial and virus strains		
E. coli OP50	Caenorhabditis Genetics Center	OP50
Chemicals, Peptides, and Recombinant Proteins		
CaCl2	J.T. Baker	1311-01
Chromalum	Sigma-Aldrich	G-1890
D-Glucose	Macron Fine Chemicals	4912-12
Fetal Bovine Serum, Heat Inactivated	Life Technologies - Gibco	10438026
Gelatin	BioExpress	9764-100G
HEPES	Fisher Scientific	BP310-500
Inulin	Sigma-Aldrich	I-3754
KCl	Mallinckrodt Chemical	6858-04
Lebovitz's L15 Media	Gibco	21083-027

MgCl2	Invitrogen	AM9530G
NaCl	Fisher Chemical	S271-500
Na2HPO4	Sigma-Aldrich	S7907-500G
NGM Plates – Lab prepared	Stiernagle, 2006 PMID:18050451	N/A
Poly-Lysine HBr	Sigma-Aldrich	P1524
SiR-Tubulin	Cytoskeleton	CY-SC002
Hoescht 33342	ThermoFisher Scientific	62249
ProLong Glass Antifade Mount	ThermoFisher Scientific	P36982
Critical commercial assays		
Invitrogen – Megascript T7 Kit	ThermoFisher Scientific	AM1334
Invitrogen – Megascript T3 Kit	ThermoFisher Scientific	AM1338
MEGAclear96 Transcription Clean-up Kit	Thermofisher Scientific	AM1909
Qiagen Qiaquick PCR Purification	Qiagen	cat. #28104
Experimental Models: Organisms/Strains		
C. brenneri	Caenorhabditis Genetics Center	LKC28
C. elegans(fog-2(q71))	CGC	JK574
C. elegans (stIs10389 [pha-4::TGF(3E3)::GFP::TY1::3xFLAG inserted into fosmid WRM0617dE06 as C-terminal protein fusion]; ltSi539[pOD1519/pSW224; Pdlg-1Δ7::mCherry::his-72::unc-54_3'UTR; Pcnd-1::mCherry::his-72::unc-54_3'UTR; cb-unc-119(+)]II; ltSi507[pOD1492/pSW201; Phlh-1::GFP::his-72::tbb-2_3'UTR, Phlh-1::mCherry::his-72::tbb-2_3'UTR; cb-unc-119(+)]IV	Wang et al., 2019 PMID: 30890570	OD1719
C. elegans (sas-4(lt127[mcherry::sas-4])III)	Ohta et al., 2021 PMID: 33399854	OD3701; insertion same as OD3702 strain used in referenced study

C. sp. 48	Marie-Anne Félix	BRC20359
C. remanei	CGC	EM464
Oligonucleotides		
Primers for *C. elegans* PAR-6 RNAi: AATTAACCCTCACTAAAGGACTGTCCGAATCATTTGCGT, TAATACGACTCACTATAGGGGACCGTCACAACAAGGAAC	Sonnischen et al., 2005 PMID: 15791247	N/A
Primers for *C. elegans* PAR-2 RNAi: AATTAACCCTCACTAAAGGGCCATTTTTCACGCAATTTT, TAATACGACTCACTATAGGGCATCAACGACGTTCAACAG	Sonnischen et al., 2005 PMID: 15791247	N/A
Primers for *C. brenneri* PAR-6 RNAi: TAATACGACTCACTATAGGGAATGGCGTCGCTTCTCAAT, AATTAACCCTCACTAAAGGGCTACGTTTCGGTGGTTTCT	This study	N/A
Primers for *C. brenneri* PAR-2 RNAi: TAATACGACTCACTATAGGACGATGGCTAAGACTGCTGA, AATTAACCCTCACTAAAGGGCGGATCGTCAAGCTGATTT	This study	N/A
Software and Algorithms		
R Studio	Rstudio	https://posit.co/download/rstudio-desktop/
Adobe Illustrator	Adobe	https://www.adobe.com/
Image J (Fiji)	NIH	https://fiji.sc/
Python(v3.12/3.12.3)	Python	https://www.python.org/
SoftWoRx Software	Cytvia	https://download.cytivalifesciences.com
Adobe Photoshop	Adobe	https://www.adobe.com/
Other		

CellVoyager CV1000- Spinning Disk High Content Confocal Microscope	https://www.yokogawa.com/	N/A
Sensoplate Plus, 384 Well, F-bottom, Glass Bottom	Greiner Bio-one	781855
Tweezers, Dumont #3	Electron Microscopy Sciences	0109-3-PO
Scalpel #15	Bard Parker	REF 371615
Zeiss Axio Observer Z1 Microscope	https://www.zeiss.com/	N/A
Nikon Ti2 Microscope	https://www.microscope.healthcare.nikon.com	N/A
DeltaVision Microscope	Applied Precision	N/A
Yokogawa CSU-X1 spinning disk	https://www.microscope.healthcare.nikon.com	N/A

830

831